Solar Energy Advances 2 (2022) 100030

Contents lists available at ScienceDirect

Solar Energy Advances

journal homepage: www.elsevier.com/locate/seja

Adapted strategy for large-scale assessment of solar potential on facades in urban areas focusing on the reflection component

Raybaud Blaise, Desthieux Gilles*

Haute école du paysage d'ingénierie et d'architecture de Genève (HEPIA), Institute for Landscaping Architecture Construction and Territory (inPACT), University of Applied Sciences Western Switzerland, (HES-SO), Geneva, Switzerland

ARTICLE INFO

Keywords:
Solar potential
Facade
Reflection
Radiosity
Photovoltaic
Urban scale

ABSTRACT

The objective of this paper is to propose an adapted method of calculation to evaluate the solar potential on building facades on a large scale. Autonomous electricity supply is nowadays an important issue, particularly during the winter. Thus the facades of buildings, which are better irradiated in winter than the roofs, can provide a response to this issue. Research has been focusing for several years on fine modeling of radiative phenomena in an urban environment. The first challenge is to obtain a physically realistic model considering the phenomena of local reflections. The second challenge is to succeed in implementing this type of simulations on large scales. These two issues are antagonistic: the first implies making the model more complex while the second implies simplifying it. This paper proposes a calculation strategy to reconcile the two issues based on a simplified radiosity method. The results obtained via this strategy were compared to those obtained by measurement and simulation on a theoretical canyon. Subsequently, this calculation strategy has been deployed to real districts in Geneva, Switzerland.

1. Introduction

Energy and climate transition face to high electricity demand, in particular through the massive development of heat pumps, e-cars and cooling systems. This results in growing pressure on the power grid, which can be linked to the current international increase in electricity prices and the risk of power blackouts. Solar energy is essential to ensure greater autonomy of urban agglomerations in their energy supply, by exploiting available local and renewable resources particularly on building surfaces.

The challenge is to integrate solar collectors as constructive elements of the building envelope (roof, façade) so that all surfaces become energy producers. This is known as BAPV (Building Applied Photo-Voltaic) or BIPV (Building Integrated Photo-Voltaic). However, the use of facades faces several obstacles: heritage, esthetic and architectural aspects, available space, significant costs, insufficient technical control. New technologies are emerging that allow the choice of colors in particular [1,2].

Another limiting factor for enhancing facades is the level of shading that is often significant in urban canyons. This phenomenon is known as the Urban Shading Ratio (USR), which can reach 60% on the façade and 25% on the roof in the densest areas [3]. If shadows are the main cause of the limited solar potential, the reflection generated between neighboring buildings can provide a significant amount of energy depending on the circumstances of the case. The challenge is therefore to reliably model solar irradiance on facades in the built environment and to detect the facade elements that can accommodate solar panels. Those elements particularly concern opaque elements not occupied by windows, even if active production technologies are emerging for glazing. Modeling tools exist for this purpose, which will be presented in part 2, but they generally address a smaller number of buildings, and are often too time-consuming to work on larger scales.

In this context, the objective of the paper is to propose a tool for modeling the solar potential on vertical facades adapted to the scale of urban centers (> 1 km^2) with reasonable computation times, paying particular attention to the reflected radiation which is the most complex component to model. The presented approach is based on tools previously developed by the authors [4–6]. These have made it possible to process the solar potential of roofs over large areas (up to 2000 km^2), as well as the potential on the facades of urban districts. However, the reflected component was processed according to a macro approach, which may not be realistic given the complexity of the phenomenon. The present paper therefore focuses on the development of a more relevant reflection modeling strategy.

The article is structured as follows (Fig. 1). Following the present introduction, Chapter 2 gives a state of the art of existing solar potential calculation models for buildings. Strength and weaknesses of each model are detailed. Then, the previous model already developed by the

* Corresponding author.
E-mail address: gilles.desthieux@hesge.ch (D. Gilles).

https://doi.org/10.1016/j.seja.2022.100030
Received 6 October 2022; Received in revised form 20 November 2022; Accepted 21 November 2022
Available online 23 November 2022

Nomenclature

CadSol	CadSol model framework for processing solar cadaster
DSM	digital surface model
DTM	digital terrain model
R-Cadsol	"Reflected – CadSol": model component integrated in the CadSol framework to process reflected irradiance on facades
SVF	sky view factor
Symbol	relevance
$I_{G,i}$	global incident irradiance on the ith scene point $[W/m^2]$
$I^0_{G,i}$	primary irradiance on the ith scene point $[W/m^2]$
$I_{D,i}$	diffuse incident irradiance on the ith scene point $[W/m^2]$
$I_{B,i}$	beam incident irradiance on the ith scene point $[W/m^2]$
R_i	incident irradiance by reflection on the ith scene point $[W/m^2]$
B	radiosity: total incident irradiance (with reflections) $[W/m^2]$
B^{tot}	received irradiance after all the reflections $[W/m^2]$
B^i	incident irradiance of the ith reflections
B^{sky}	incident irradiance projected on the sky mesh
Symbol	relevance
ρ	reflection coefficient
ρ_g	ground reflection coefficient
β	tilt angle of the plane
S_i	surface area associated to the ith scene point
dS_i	infinitesimal variation of the variable S_i
θ_i	angle of incidence on the scene point i
E	initial incident irradiance $[W/m^2]$
F	form factor matrix
$r_{i,j}$	distance between scene points i and j $[m]$
$\overrightarrow{n_i}$	normal vector on scene point i

authors, CadSol, is presented in a Chapter 3. This introduces Chapter 4: the development of the new model component, R-Cadsol for a more reliable and accurate modeling of the solar reflection at large scale based on radiosity. A validation of the model is detailed in Chapter 5 and Chapter 6 presents the results on a real scene. Chapter 7 concludes the paper by some discussion and perspective words.

2. Review of the existing models

Several models can be used to calculate urban irradiance at different scales and with different degrees of accuracy. Solar potential calculation models must meet two requirements: a sufficiently large-scale calculation with a reasonable calculation time. Different calculation strategies exist, seeking to balance between physical accuracy, scale of analysis, complexity and ease of use while considering computer constraints.

Table 1 provides a comparative view of the most common solar models based on information from the literature review.

The models are compared and filled in according to the following fields:

- Model: name of the model;
- Author: the institution that developed the model;
- Date: launching year;
- Quick description of the model based on the website of the model/institution and the references in the literature.
- Adapted scale of the model based on the known practice of the model and the references in the literature. The scale of use of these models goes hand in hand with their spatial accuracy, the resolution of the used urban model, the spatial unit (cloud of scene points or meshes) and the computing performance. The considered scales are the following: (i) block of buildings, i.e. a couple of buildings in a small space area (less than 500 m2), which means building and its closest neighbors, (ii) district, i.e. urban area ~1 km2, (iii) large scale on several square kilometers.
- Methodology: if facades (in addition of building roofs) are computed, if yes with which method for the reflection component.

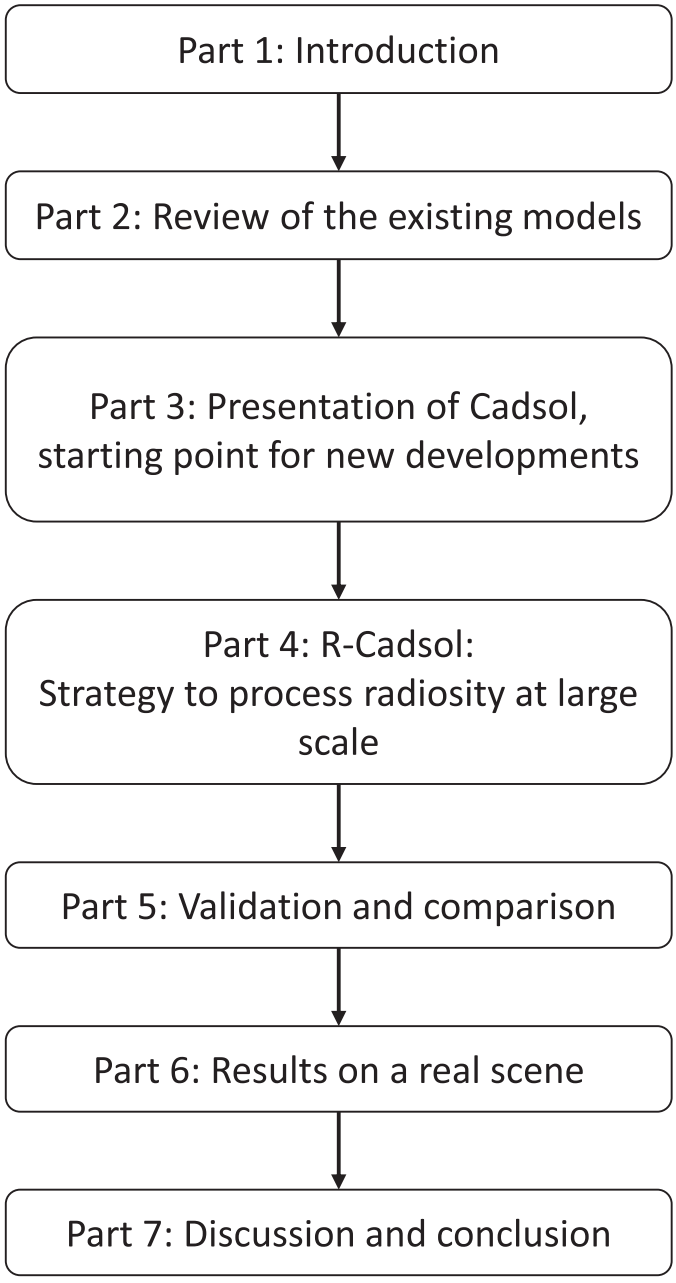

Fig. 1. Structure of the article.

Most models can handle district scale computation, but large-scale computation considering reflections, whatever the method used (radiosity or ray tracing), is still a challenge today.

A benchmarking study was carried out between CadSol and many of the listed models in this chapter [23,26]. The study dealt with typical days in winter and summer on theoretical blocks of buildings based on the same hourly weather data. Compared tools showed similar hourly radiation results on facades and roofs. But tools that address building scale propose finer spatial variation patterns along the facades, due to smaller computation time scale and a large number of specific parameters.

Table 1
Overview of the main models for assessing the solar potential in urban areas (large scale: about 1 km2, district scale: a few buildings). Other models not presented here because they are not widely used or have been abandoned. Those models are detailed in [25].

Model	Author	Date	Quick description	Adapted Scale	Methodology
CitySim	EPFL / LESO-PB	2003	CitySim is based on a simplified radiosity model (SRA) [7]	Large scale [8]	Radiosity
SOLENE	Creneau – Laboratoire AAU	2000	Calculations of sunshine at the neighborhood scale taking into account solar reflections by radiosity method [9]. This tool is now used by SOLENEOS to analyze urban heat islands [10].	Block of buildings [10]	Radiosity
Grasshopper Honeybee	Ladybug tools	2016	This model can be seen as the Ladybug model enriched with a consideration of solar reflections [11]. Reflections are calculated using ray tracing algorithm, in particular the Radiance software.	District	Ray Tracing
Grasshopper Daysim	MIT	2001	Daysim is a software dedicated to urban solar radiation calculations based on a ray-tracing strategy [12]. It uses Radiance as a calculation engine. Solar reflections on surfaces are evaluated.	District [13,14]	Ray Tracing
Grasshopper Diva	Solemma	2008	Design Iterative Validate Adapt (DIVA) is a black box plug-in that fits into the Rhinoceros software. It processes sunshine according to a method using the Radiance software. This method of calculation is coupled with the precision of the Rhinoceros and considers complex geometries.	District [15,16]	Ray Tracing
Climate Studio	Solemma	2020	ClimateStudio is the black box software currently offered by the company Solemma. The sunshine calculation model has a similar operation to DIVA and then using Radiance	District	Ray Tracing
Archelios Map	TraceSoftware	2019	Black box software that allows to calculate sunshine maps on roofs from 3D models and to manage solar PV projects. The cast shadows are taken into account but not the solar reflections on surfaces [18]	Large scale	Facades not computed, global irradiance (no reflection modeling)
Smart City Energy	LIST	2019	The Smart City Energy Platform [19] supports cities to develop new strategies and opportunities for sustainable energy transitions. In particular, the authors [20] developed a forecasting model for Luxembourg, able to predict the expected regional PV power up to 72 h ahead.	Large scale	Facades not computed, global irradiance (no reflection modeling)
Grasshopper Ladybug	Ladybug tools	2013	Ladybug provides climate graphics based on weather files and supports solar radiation studies, view analyses, and sunlight-hours modeling. It is embedded within the visual programming language environment Grasshopper, linked to Rhino3D [21]. Only cast shadows are considered [11].	District [17,22]	No reflection modeling
CadSol	HEPIA	2018	Model used for the solar cadaster of Geneva for roofs, floors and facades [5,6,28].	Large scale	The consideration of reflected radiation is approximate based on Iqbal model [24]

In general, the larger the processed area simulation is, the less precisely the optical properties of reflections are modeled. The constraint behind this choice is usually a computational time constraint. Then, none of the proposed models allows the calculation of urban solar cadasters with the required geometric finesse and the desired accuracy on optical reflections. Archelios map and CadSol are the only models that allow the calculation of large-scale solar cadasters. However, Archelios does not consider the solar reflections nor process solar potential on facades, while CadSol is based on approximate model of reflection (see 3.2.2). In CadSol, cities and regions are not processed as a whole, but trough a set of 3 × 3 km tiles (actually 3.2 km considering mutual shadowing between tiles over a distance of 200 m).

Faced with this observation, this article proposes an improved version of the CadSol model based on an adapted and adequate model of reflections, with the objective of finding the best compromise between a reliable calculation of the reflection and the analysis of the solar potential on a large scale.

3. CadSol

3.1. Workflow

The CadSol tool [5] has been using for more than 10 years to process and update the solar cadaster of the roofs of the Canton of Geneva [5,6]. The solar cadaster was recently extended to the Greater Geneva [4,27]. A Web application [28] was also developed to allow any owner to view the solar potential on the roof and simulate the self-consumption of solar PV.

A workflow of this tool is introduced here including the improvement proposed in this paper concerning the modeling of optical reflections (Fig. 2 red box). The different calculation steps of the CadSol model use different software and computer languages as highlighted by the colors. The original CadSol model is able to calculate irradiances on very large scale, but without taking into account reflections from the built environment in appropriate manner. The purpose of the R-Cadsol model is to thus to fill this gap.

The following sections present a detailed review of the calculation steps of the original CadSol model providing the input variables for the optical reflection model.

3.2. Integration of the scene

As presented in [6], the DTM and DSM data are derived from LIDAR field surveys. The frontage points are deduced from the difference in altitude between the DTM and DSM models with an arbitrarily defined step in space. Such models are described as 2.5D models with a simplified geometry compared to reality, especially on the facades, which are then flattened. The facades also have a default slope of 90° without considering overhangs, and homogeneous azimuth, which is attributed to each point along the facade. Particular cases like rounded faces will be modeled using the DSM that enables to consider slope variation. Because of the formats of these files, it is easier to work with a scene composed of cloud of points and not of meshes. Building a mesh network from the scene points is indeed complicated. The difficulty lies in ensuring that all the meshes are joined throughout the scene and that the generated surfaces are consistent with the surfaces of the real scene. This is a

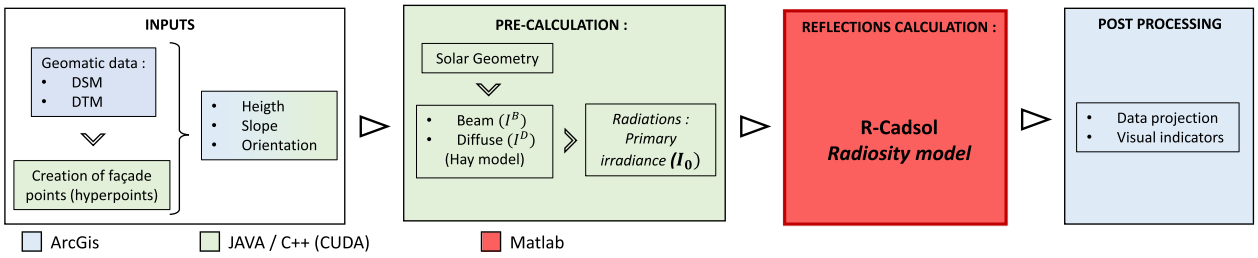

Fig. 2. Global CadSol workflow for the calculation of solar radiations on roof and façades including reflections.

mathematical problem not studied in this project. The choice was then made to find a solution allowing to work on the cloud of points.

3.3. Sky model and shadow casting

The Eq. (1a) presents the global incident irradiance on the ith point ($I_{G,i}$), from direct or beam incident radiation ($I_{B,i}$), diffused incident radiation ($I_{D,i}$) and reflected incident radiation (R_i). The Eq. (1b) introduces the primary irradiance, composed by the beam and diffuse components only, as the main input of the radiosity calculation (see Chapter 4.3).

$$I_{G,i} = I_{B,i} + I_{D,i} + R_i \tag{1a}$$

$$I^0_{G,i} = I_{B,i} + I_{D,i} \tag{1b}$$

3.3.1. Beam and diffused irradiance

As detailed in [6], the modeling of the primary irradiances (beam and diffuse) is performed using an open source model encoded with JAVA. This latter has been then moved to C++ and CUDA in order to improve computing performance using a GPU machine [4] and process large areas like the Greater Geneva (2000 km^2).

Primary irradiances are calculated on facades and/or roofs. Direct and diffuse source irradiances on horizontal surface are derived from statistical meteorological data (using the database Meteonorm®). Shadow casting for Sky View Factor (SVF) and hourly shadow on the beam component are calculated adapting the model proposed by Ratti in his thesis work [29].

A first calculation allows to determine the direct incident irradiance from the coordinates of the DSM points and the position of the sun. The position of the sun is determined from the elevation and azimuth angles. The irradiance on a horizontal surface is transposed from the angle of incidence determined between the direction of direct rays and the normal to the surface.

Concerning the diffused radiation and SVF, the same calculation routine is used. It is however repeated on 580 positions of the light source defined by default whose light intensities are calculated using the Hay model [30]. The results from these 580 sources are then aggregated to obtain SVF and then the incident diffused irradiance.

The difficulty in urban areas lies in the identification of the R_i value for each point. This is the objective of the model detailed below.

3.3.2. CadSol original reflections calculation

CadSol, in its original version, uses an isotropic approach to calculate the irradiance from reflections [24,31]. β is the plane tilt angle and ρ_g the ground reflectance (albedo).

$$R_i = \left(I_{B,i} + I_{D,i}\right) \rho_g \left(\frac{1 - cos\beta}{2}\right) \tag{1}$$

The reflection received by a given tilted surface is thus a fraction of the sum of the beam and diffuse irradiance, which is multiplied by the albedo representative of the surrounding environment and a cosine function of the surface inclination. Therefore, if the tilt angle is null the reflection will be null too, the reflection will be maximum in the case of a vertical surface.

The main shortcoming of this model is that the local urban geometry is not considered, whatever it is an open area or an urban canyon for instance. Therefore, for any point of a facade regardless their position (height), the solar irradiance provided by reflection will be identical. Shading analysis (interruption of the ray between two points by an obstacle) is not addressed either. If this approach has provided so far a helpful support in the original CadSol model to estimate large-scale reflection very quickly, the aim here is to propose a more realistic and reliable strategy on reflection modeling, taking into account the geometry properties of the surrounding built environment.

4. New strategy for calculating reflections in CadSol model

The model is at this stage a prototype developed in Matlab and aims to improve the CadSol model concerning reflection modeling. We integrate thus in the CadSol framework a new component 'R-CadSol' (see Fig. 2) dedicated to the reflection calculation using radiosity approach.
.

The objective of this model is to succeed in reconciling reliable calculation of reflections on facade with calculations on a large urban scale of at least 1 km^2.

4.1. Introduction to radiosity modeling

The proposed R-CadSol model uses a radiosity method, which allows to compute the diffuse reflections on all the surfaces composing the urban scene. Radiosity is based on an energy balance calculation and is written as a linear algebra problem. Usually, this method requires a mesh network of the urban scene. The representative equation for the classical radiosity method is presented in Eq. (2). B is the radiosity, which is the total irradiance incident ($[W/m^2]$) on each of the meshes composing the urban scene, F is the form factor matrix, and ρ represents the vector of reflection coefficients, where ρ_i is the reflection coefficient of mesh i. E is the source term, with E_i the irradiance initially received by mesh i ($[W/m^2]$).

$$B = E + \rho F B \tag{2}$$

The main difficulty using a radiosity method is that the calculation is representative of all radiative exchanges from mesh to mesh. Therefore, it is necessary to store information for each pair of meshes. This information is called "Form Factor" and is generally noted $F = (f_{i,j})_{1 \le i,j \le N}$. It represents the "perception of the mesh j from the mesh i" and is calculated as described in the Eq. (3). Fig. 3 provides an illustration of the concept of the form factor.

$$F_{i,j} = \frac{1}{S_i} \int_{S_i} \int_{S_j} \frac{cos(\theta_i)\cos(\theta_j)}{\pi r^2_{i,j}} dS_i dS_j \tag{3}$$

The objective here is to reduce the dimension of the problem and to find an alternative to this mesh-by-mesh calculation in order to save computing time and data storage necessary for large urban areas. The approach proposed is based on the Nusselt analogy [33] and similar

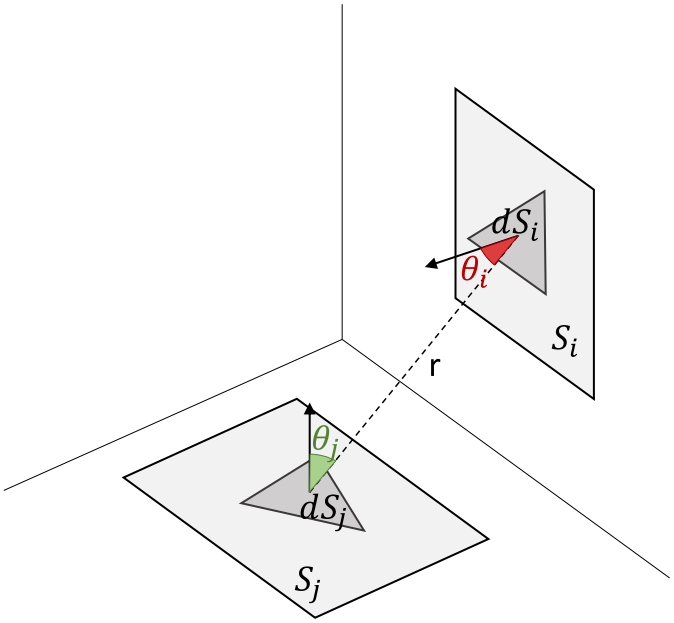

Fig. 3. Illustration of the notion of form factor: visibility between meshes (adapted from [32]).

to the one used in the work of Cohen et al. [34] where the meshes j composing the surrounding scene are projected on a half cube centered on the study mesh i. However, we suggest to use a sphere instead of the hemicube (Fig. 4) to facilitate homogeneous solid angles in all directions and to avoid sampling density problems. This strategy has already been used in recent studies where heat propagation needs have to be known [35].

Fig. 4 illustrates the computational process. Each point of the scene model (red dot) is assumed to be included in a 1 m^2 square mesh. The computational sphere and the associated meshes are centered on this point. Each mesh of the sphere (red triangle) is projected on the scene (green triangle) in order to obtain a discretization of the scene visible from the red point. In the rest of the paper, we will distinguish the "sky meshes" (the meshes of the sphere) and the "scene points" (the center of square mesh).

Because of its mathematical construction, radiosity presents the disadvantage of only modeling Lambertian reflections. Indeed, reflections are calculated without considering the incident angle of the rays. Specular reflections [36], especially in the case of significant incidence on glass surfaces, cannot be modeled without adaptations considering the incident angle of the rays, such as ray tracing [37]. In the following, 2968 sky meshes from the sphere are considered.

4.2. Calculation of the primary irradiance (without reflections)

The direct (I_B) and diffuse (I_D) sunlight on each scene point are provided by the CadSol model (pre-calculation component) as presented above in Section 3.2.1 and Fig. 2. It allows to calculate the primary irradiance on the scene (I_G^0) as defined by the Eq. (1b).

4.3. Adapted radiosity method on a large scale: calculation of successive reflections

The irradiances are calculated for each point of the scene (ground, facades and roofs). The reflection calculation strategy is based on the use of a sphere centered successively on each point of the scene. Each point being located on a surface of the scene, only the half-sphere located on the outside of the surface is considered. Before the calculation of reflections, a pre-calculation via the Cadsol model is performed. This calculation allows to determine the primary irradiance (I_G^0) on each point. The primary irradiance already takes into account the date and time of the calculation, the orientation of the surfaces and possible masks.

By using a bounding sphere, the interest here is to filter the number of directions to explore and identify the elements visible from each point. The radiosity is then calculated between the scene point and the sky mesh (instead of scene point to scene point in order to decrease the memory storage and boost computation time). This requires the projection of the scene irradiances on the sky mesh and then rewriting the Eq. (3). The form factor matrix F is no longer square and therefore invertible. An iterative strategy is required to obtain the irradiance after n reflections (Eq. (4) and Fig. 5). For the calculation of the first order reflection, the primary irradiance on the scene (I_G^0) is projected on the sky mesh according to the mesh directions and for each scene point. The matrix defined by $\rho_{S.} * B^{0,sky}$ is then created, where each column is the projection of the scene reflected irradiances on the sky meshes. Each column is representative of a centered sky sphere on the point i. It explains why only the diagonal is kept: the calculation of $diag(F(\rho_{S.} * B^{0,sky}))$

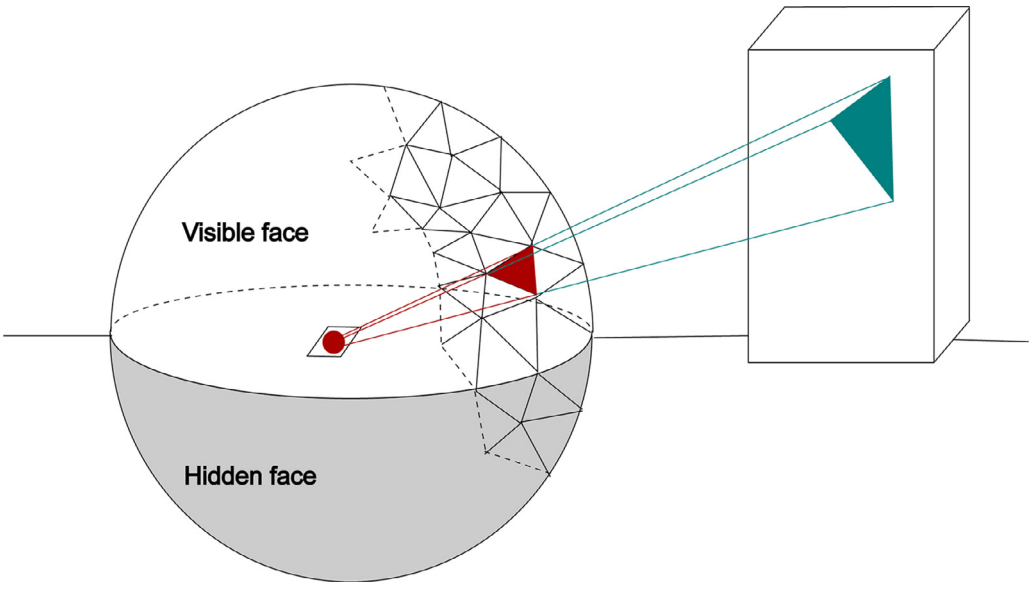

Fig. 4. Representation of the enclosing sphere from which the form factors are calculated.

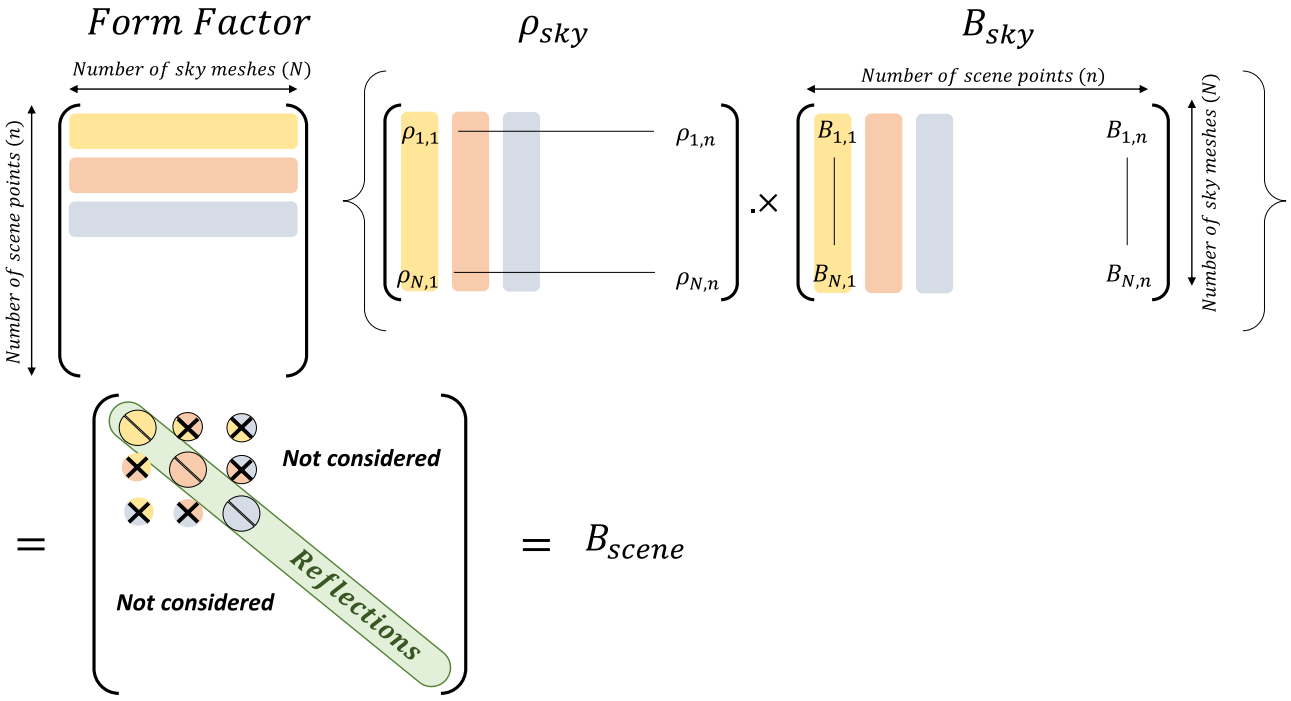

Fig. 5. Schematic representation of the calculation strategy. Matrices are called "ρ_{sky}" and "B_{sky}" because they contains values for couples "sky mesh – scene point". Only the diagonal is considered in the final result.

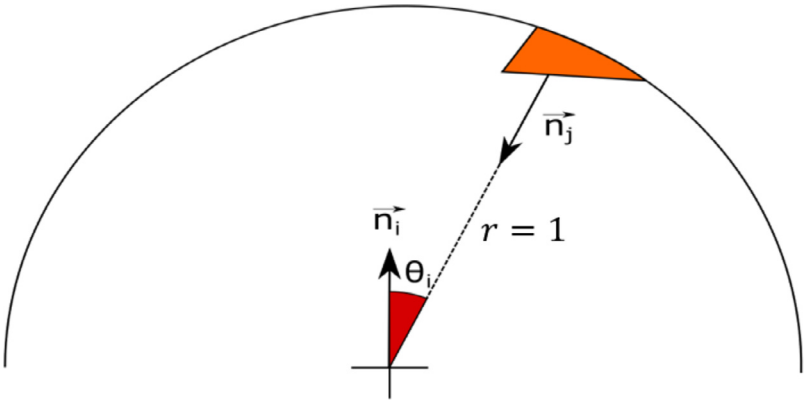

Fig. 6. Cross-section of the enclosing sphere and the considered angles.

gives a vector of the incident irradiances on the scene point. These operations are repeated at each reflection order, where only the new reflection is calculated.

$$\begin{cases} B^0 = I_G^0 \\ B^1 = diag\left(F\left(\rho_S . * B^{0,sky}\right)\right) \\ \cdots \\ B^n = diag\left(F\left(\rho_S . * B^{n-1,\ sky}\right)\right) \end{cases} \tag{4}$$

The total incident irradiance B^{tot} on each scene point is therefore the primary irradiance incident B^0 on the scene plus the sum of the successive reflections (Eq. (5)).

$$B^{tot} = \sum_{k=0}^{n} B^k \tag{5}$$

The calculation of the form factors is based on the same formula as given in Eq. (3). However, the use of the bounding sphere shown in Fig. 4 simplifies the formula. Indeed, based on the original equation we can perform the following calculation: Eq. (3) can be simplified assuming that $r = 1$ and $\theta_j = 90°$ (Fig. 6). We then obtain the Eq. (6).

$$F_{i,j} = \int_{S_i} \int_{S_j} \frac{\cos\left(\theta_i\right)}{\pi} dS_i dS_j \tag{6}$$

Assuming that the mesh size of the sphere is fine enough, and the angle θ_j is close to 0 for all the sky mesh j, we can make the following approximation (Eq. (7)):

$$F_{i,j} = \frac{\cos\left(\theta_i\right)}{\pi} S_j \tag{7}$$

In practice, the form factors sum should not exceed 1, so as that no additional energy is created over reflections. To ensure this condition with the assumptions used, the form factors are then normalized by their sum (including sky meshes and scene points). This normalization is a priori useless, but it allows to avoid numerical errors and irradiance peaks in closed corners with high intensity of reflections and with form factors that can be close to 1, or even slightly exceed 1.

5. Validation on theoretical urban canyon

A canyon mock-up of 2.6 m long, 0.6 m wide and 0.6 m high was built as part of Raybaud's thesis [25], in order to compare measurements

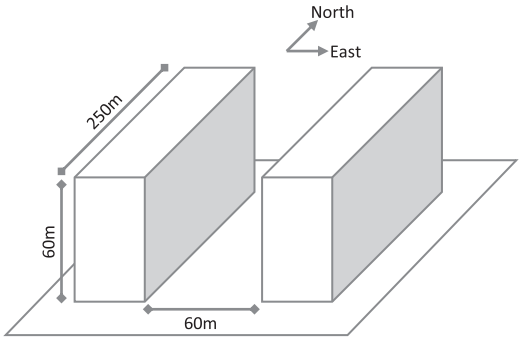

Fig. 7. Urban canyon on which comparisons between the classical radiosity model and the modified CadSol model are conducted.

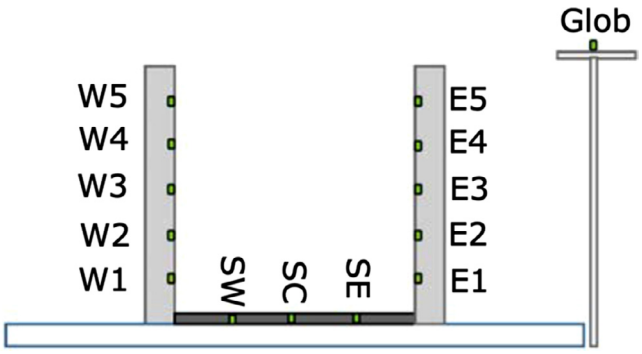

Fig. 8. Geographical location of the control points in the canyon (E = East, W = West, SW = Soil West, SC = Soil Center, SE = Soil East, Glob. = Global).

and simulation based on identical height/width ratios of the canyon. Several scenarios were compared considering materials with different albedo properties on each façade. The results presented in the thesis showed the relevance of a radiosity-based strategy to simulate solar irradiances.

It is therefore consistent to compare the R-CadSol model to the classical radiosity model built in Raybaud's thesis. The digital scene, keeping the same proportions of the mock-up, corresponds to a 250 m long, 60 m high and 60 m wide canyon (Fig. 7). To facilitate the comparison between the performance of the models, the direct and diffuse radiations from the thesis are used as inputs in the R-CadSol model: for each point of the R-CadSol scene, the affected radiation corresponds to the one of the mesh (mesh from the thesis) in which the point is centered. The reference day is a virtual day, representative of typical weather conditions, that was considered in the thesis (May 19, 2019). The control points shown in Fig. 8 aim to visualize the evolution of the irradiance over time. They are located at the canyon's center, at 10, 20, 30, 40 and 50 m height, respectively, in order to be less sensitive to edge effects, in particular to irradiances coming from the extremities of the canyon. Three control points are added on the ground.

5.1. Form factor validation

The form factors obtained with the R-CadSol model are compared to the theoretical form factors obtained with standard radiosity. As the form factors are calculated mesh by mesh in the work of Raybaud it is impossible to compare each form factor on a case-by-case basis. Therefore, the validation follows two steps: (1) we compare the sum of the form factors for each scene point; (2) to make the comparison geographically, the form factors calculated in the R-CadSol model are interpolated on the control points of the thesis. These points correspond to the barycenter of the meshes of the thesis.

We note in Figs. 9 and 10 that the form factor calculation in R-CadSol gives similar results to the classical calculation method. The standard deviation is mostly positive with a larger absolute deviation for positive values (Fig. 9), then it appears at this point that the R-Cadsol model slightly overestimates the form factors. Large discrepancies (more than 5% difference on the form factor value) are noted on less than 5% of the scene points. These discrepancies are observed at the level of discontinuities (angles) in the scene (Fig. 11), especially at the north and south ends on the edge of the canyon. This is due to the proximity of the scene edges which can generate different boundary conditions with a high variability on the intersection of a point or not, especially when a point is close to a facade with a high value of incidence.

These results validate the simplified method of the form factor calculation as introduced by the R-CadSol model. It is now necessary to validate the strategy of calculation of solar irradiances.

5.2. Irradiance validation

The Fig. 12 shows a comparison of the irradiance results from the thesis (classical radiosity model with lambertian reflections; all reflections are modeled with albedo coefficient of 0.7 on each façade and 0.3

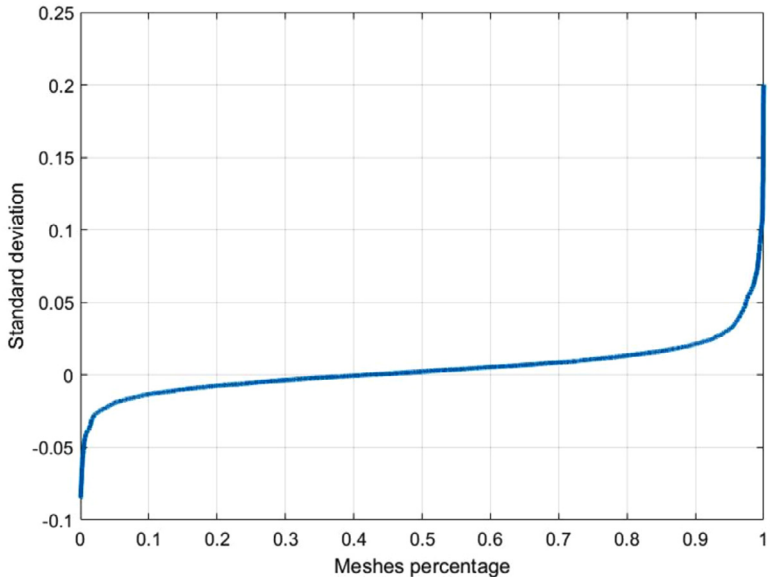

Fig. 9. Distribution of relative errors ((R-Cadsol - Thesis)/max(Thesis)) as a function of the form factor calculation method. The number of points is reduced to a percentage value of the total number of points.

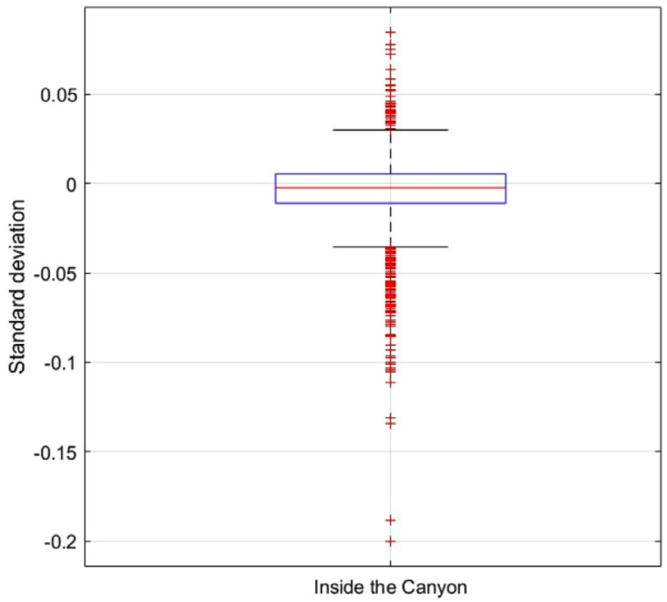

Fig. 10. Boxplot of relative errors as a function of form factor calculation mode. This box plot only deals with the control points inside the canyon shown in Fig. 8.

on the ground) and those obtained with the R-CadSol model (with same parameters and three reflection orders). This comparison is carried out on the control points for a typical day, as mentioned earlier, in order to avoid the variabilities linked to meteorological instabilities, especially clouds. It corresponds to an ideal clear day with an exact trajectory of the sun. This results in a perfect continuous line corresponding to the sunlight curve (black curve on Fig. 12).

Fig. 12 shows that the results obtained from the R-CadSol model are very similar to those obtained in Raybaud's thesis. We observe a maximum difference of about 20 W/m^2 between the two models, with a lower irradiance for R-CadSol which can be explained by not considering all the reflections (only the first three reflections are considered). We can therefore conclude that the two models are globally in good agreement on irradiance results.

6. Results and application on a real urban scene

The developed model is tested on a real scene, the Meyrin district located in the northwest of Geneva. This area is interesting because it presents relatively well-spaced and regular buildings with blind gable walls which could be equipped with photovoltaic modules (Fig. 13). The main facades also offer many opaque surfaces which can be used for PV installations. The primary irradiance are calculated from the CadSol model (pre-calculation of beam and diffuse components, see Fig. 2). The different masks (buildings, trees, …) are considered. Then the R-CadSol model enables to process the reflection component and finally the global irradiance.

Table 2
Albedo values for each type of surface [38,39].

Id	Surface	Albedo	Association
1	Other hard surface	0.3	Aged concrete
2	Other green surface	0.25	Green grass
3	Building perimeter	0.3	Aged concrete
4	Forest area	0.18	Deciduous trees
5	Building, type 1	0.3	Aged concrete
6	Parking space	0.12	Aged asphalt
7	Pathway	0.33	Tar & gravel
8	Building, type 3	0.3	Aged concrete
9	Swimming pool	0.1	Water
10	Bush	0.18	Deciduous trees
11	Pavement	0.3	Aged concrete
12	Parking	0.33	Tar & gravel
13	Cycle path	0.12	Aged asphalt
14	Roadway	0.12	Aged asphalt
15	Building, type 2	0.3	Aged concrete

6.1. Albedo mapping

The scene is $300m \times 300m$ and is meshed with a resolution of 0.5 m. The points generated on the ground, roof and vertical (facades) surfaces constitute a set of 685,624 points. Reflection coefficients are assigned for each surface according to the material identified (Fig. 14). This information is taken from the coverage data of the Territorial information system of Geneva (SITG, see https://ge.ch/sitg/). Albedo factors are assigned to each type of coverage and detailed in Table 2.

6.2. Form factors

Considering 2968 sky points, the form factor matrix occupies an approximate memory space of 1.02GB when stored in single type (i.e. 4 bites for one data), which is particularly important. The calculation of form factors allows to perceive the impact of other buildings on each study point (Fig. 15). Points where the sum of the form factors is close to 1 signify a strong influence of masks whereas a sum close to

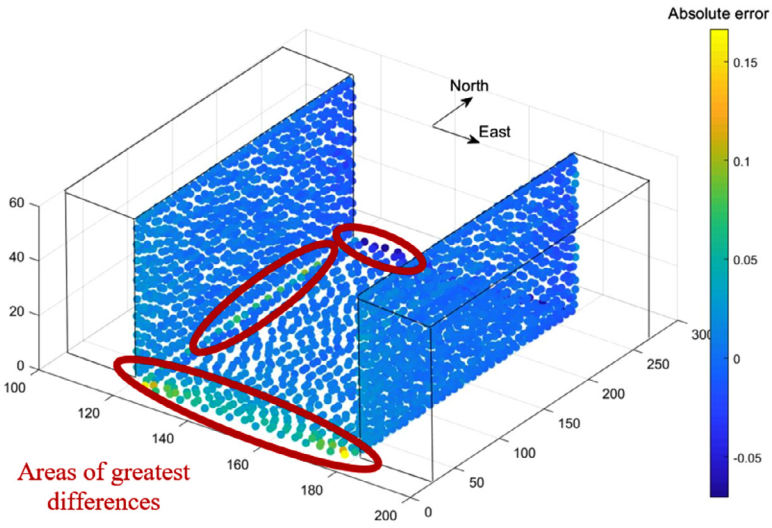

Fig. 11. Visualization of the differences between the form factors calculated with the adapted model and the exact projected form factors (by interpolation).

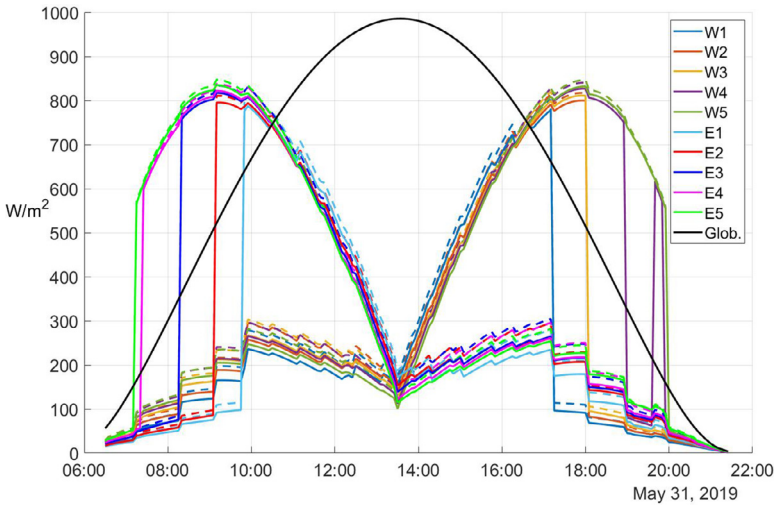

Fig. 12. Comparison for all control points between the results from the Raybaud's thesis (dashed line) and the results from the VALES model (continuous line).

Fig. 13. Image of the Meyrin district extracted from Google Maps.

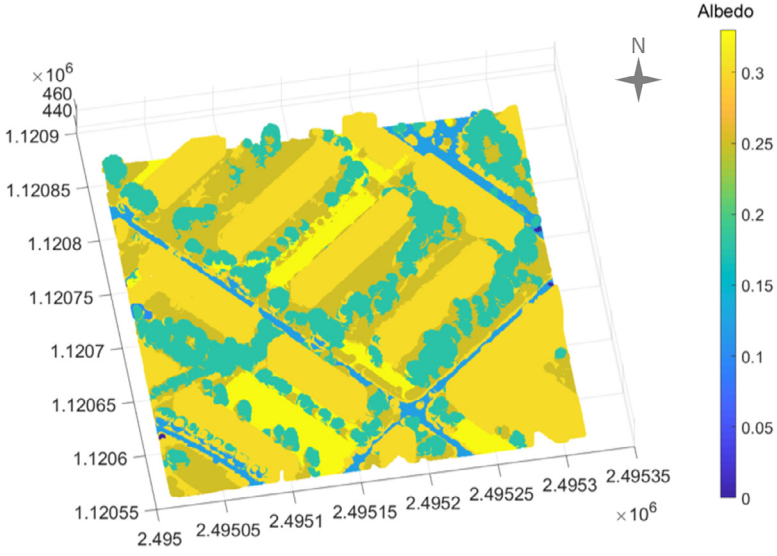

Fig. 14. Projection of the albedo values.

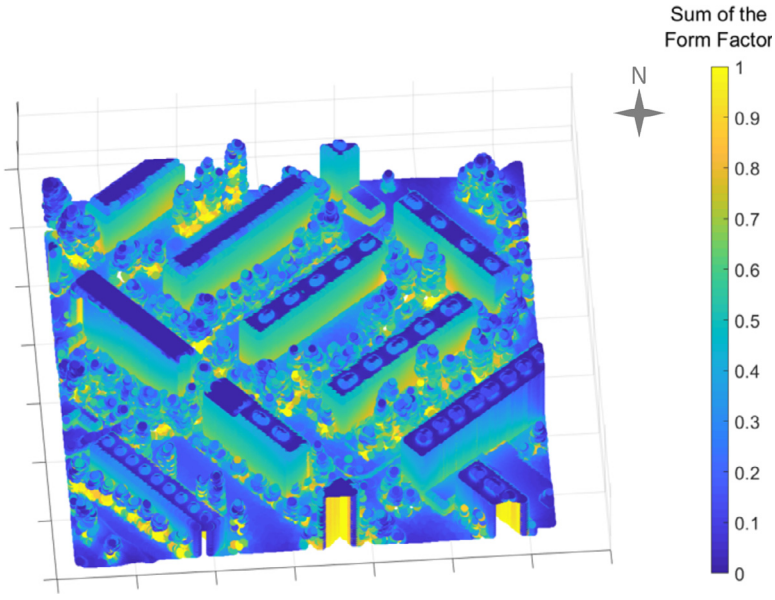

Fig. 15. Calculation of form factors in the Meyrin district.

0 indicates high visibility of the sky. The sum of the form factors is then the inverse of the sky view factor.

For reasons of memory storage and calculation time, only the first two reflection orders are calculated. In extreme cases (with favorable geometry and high albedos of 0.9), the error between the model using two reflection orders and reality can be estimated between 15 and 20% on facades not exposed to direct sunlight [25]. In reality, the relative error is generally smaller although it is difficult to quantify it, because it depends on the geometry and material properties. In the case of our configurations considering albedos of 0.3 on facades, this error should not exceed 5% because it remains 9% (0.3×0.3) of energy after two reflections and we assume that only half of this lacking energy would be recovered by the scene.

6.3. Irradiance analysis

We present the results of the irradiance analysis on this real scene, the primary irradiance (beam and diffuse) and the specific contribution of the reflection component on surfaces. Weather data are based on Meteonorm® (see https://meteonorm.com/en/) that provides representative statistics for a given location as introduced in Chapter 3. This demonstration is made for a given hour which is 12:00 CET on 1st May.

Fig. 16 shows the primary irradiance at this time. The position of the sun is relatively high in the sky, which results in low cast shadows. In Fig. 17, very important reflected irradiances are noted locally. They come from side-effect phenomena, at the level of strongly masked points whose form factors are close to 1, especially in trees. We also observe on this map that the contribution of reflections is consistent, about $120 W/m^2$, at the base of the south/west and south/east facades. The effect of nearby masks is also apparent, especially on facades covered by trees. Finally, as pointed out in Fig. 17 (red circle), edge effects are visible on buildings truncated on the edges of the map.

Fig. 18 displays the global yearly solar irradiance on the studied scene on roofs and facades. We are interested in assessing the specific contributions of facades and reflections based on time and spatial variation. The comparison is performed on two points: a flat and unshaded roof and a southeast facade of building located at 13 m height over a total height of 17 m (red points Fig. 18). The first analysis is to compare hourly irradiance on facade and roof points, and hourly reflection on global irradiance. Fig. 19 thus shows the hourly profiles of global and only reflected irradiances on the roof and facade points. The solar

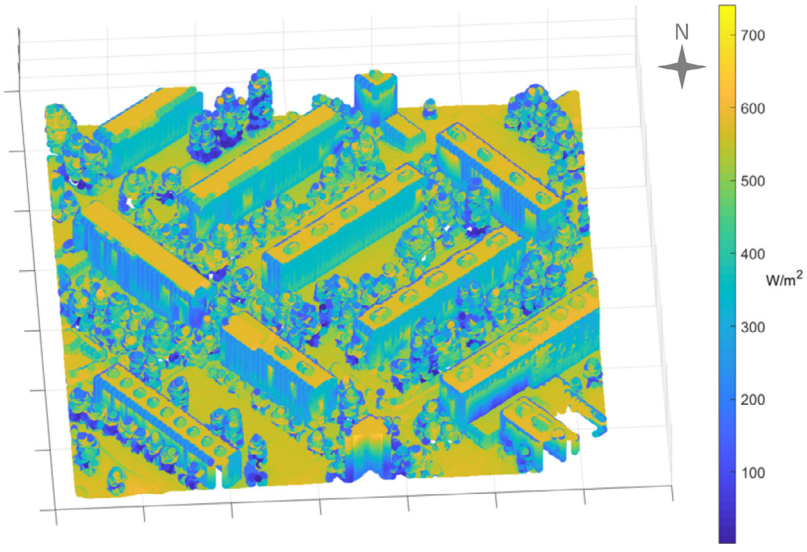

Fig. 16. Solar gain from primary sunlight (direct and diffused) in the Meyrin district on 1 May at 12:00 UTC. North corresponds to the y axis.

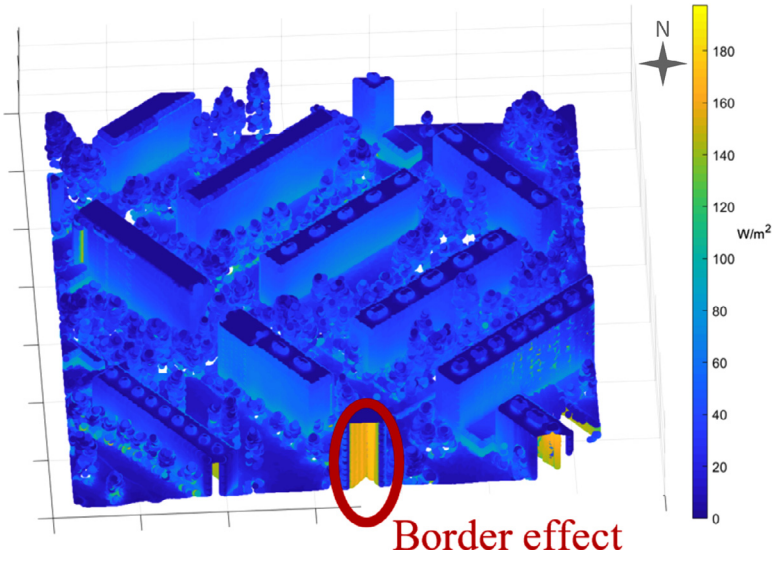

Fig. 17. Solar contribution from the reflections on the Meyrin district on 1 May at 12:00 UTC. North corresponds to the y axis.

potential on the facade appears to be higher from October to March. In winter, the maximum difference is observed in February where the solar potential reaches 300 W/m^2 on the roof whereas it reaches more than 400 W/m^2 on the southeast facade. This observation is consistent with the role of the well-exposed facades in order to improve solar electricity supply, particularly in winter where demand is higher and renewable energy sources are less available.

Secondly, it is interesting to observe the hourly profile of the reflection only. On the roof point, reflection is nearly zero all year long as this roof is flat, unshaded and is not visible from almost any other point in the scene. On the facade point, the contribution of reflection is higher in summer (40% of the total irradiance) than in winter (20%) as also shown by Fig. 20. This is because the sun position is lower in winter and the facade receives more direct radiation, on the contrary in summer the sun is higher which impacts more on reflection from the ground. In addition, reflection depends on the quantity of the primary irradiance (direct and diffuse) which is higher in summer. From Fig. 19 we also observe a delay between the peak of the total irradiance on the facade (around 12 pm) and the peak of the reflected as well as that of the global irradiance on the roof (around 1 pm). The reason is that the facade is slightly oriented to the east, and thus the peak intervenes earlier than on flat surface (ground, as the main source of reflection, and roof).

The following two figures (Figs. 21, 22) display the yearly irradiance profile along the façade corresponding to the red dot point (Fig. 18) from the roof to the ground with an interval of 1 m. They distinguish the contribution of the primary irradiance (beam + diffuse) and that of the reflection, the sum of the two contributions corresponds to the global irradiance. We can note that as we go lower the reflection becomes more important due the reflection from the ground, as it was already observed in Fig. 17 for a given day. On the contrary, as we go higher direct and diffuse increase due to less shadowing from neighbors.

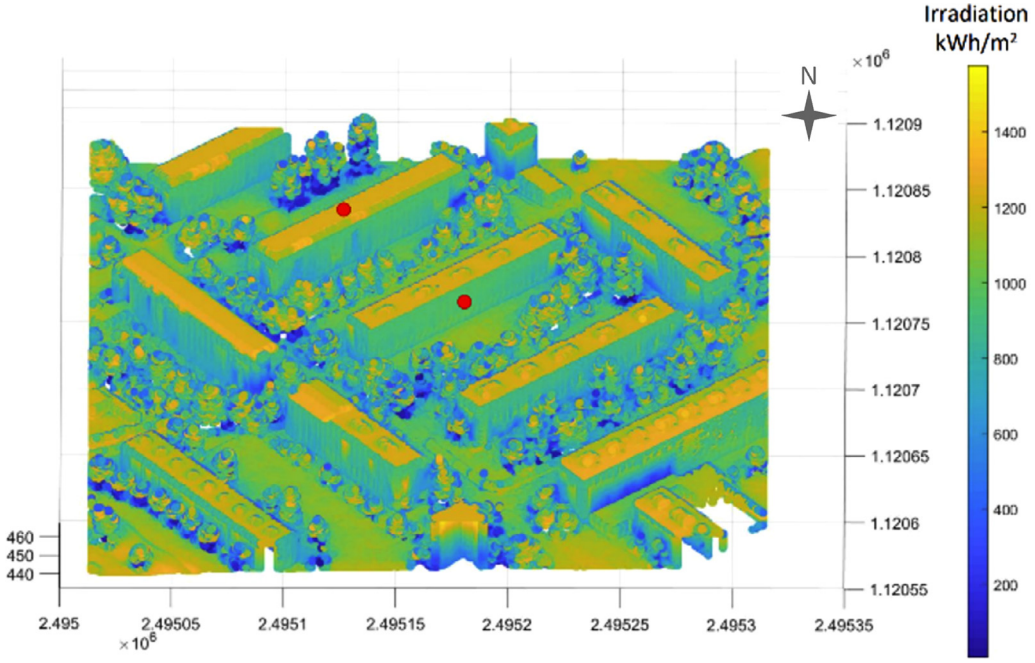

Fig. 18. Annual solar irradiance (kWh/m^2) on the Meyrin district with the two studied red points.

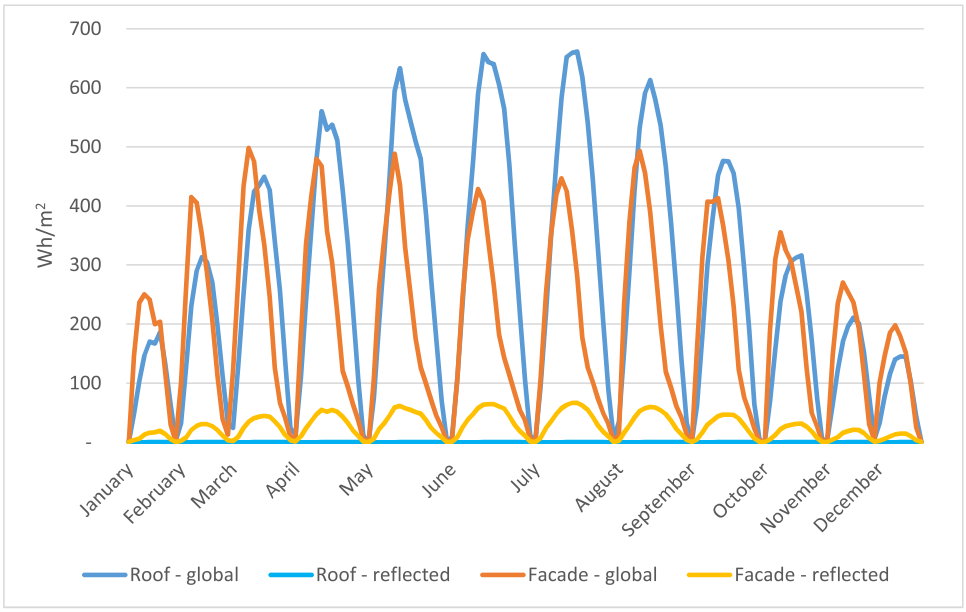

Fig. 19. Hourly profiles of global and reflected irradiance (W/m^2) on the two studied points – roof and facade.

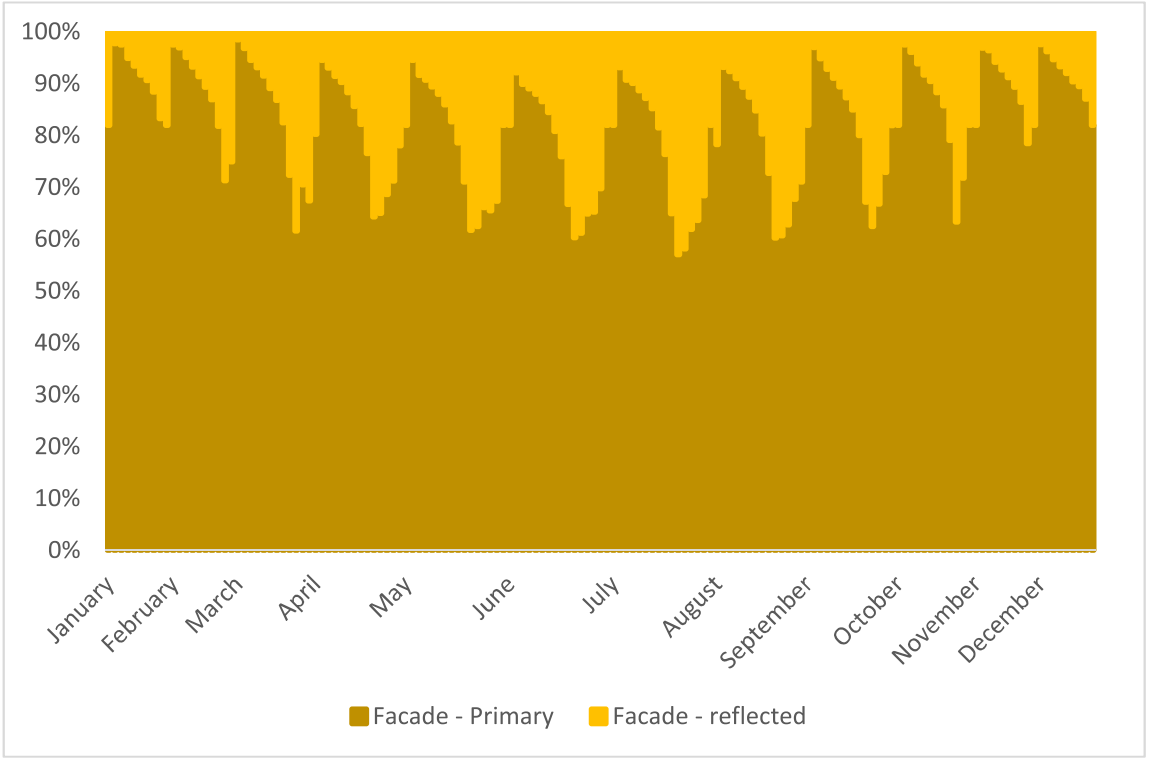

Fig. 20. Hourly profiles of primary and reflected irradiation in% on the studied facade point.

7. Discussion and conclusion

This paper proposed a prototype of a solar irradiance calculation algorithm based on an adapted radiosity algorithm, and showed the potential to calculate reliable solar reflections on large urban scale. An example presenting the use of the model on a real neighborhood (Meyrin) at a scale of 300 m x 300 m and with a resolution of 1 m is presented. Only the first two reflections are calculated.

This radiosity adapted strategy, implemented to the R-CadSol model, has been validated comparing the results with the classical radiosity strategy. Differences on form factors appear only on less than 5% of the meshes and the absolute difference on irradiance between the models is lower than 20 W/m^2, which is very satisfying. Although the model is still a prototype coded in Matlab, it can already produce sound results for 300 m x 300 m neighborhoods (district scale) with a 0.5 m a vertical and horizontal resolution for the whole year.

Despite the results of the comparison between the classical radiosity approach and the simplified method introduced in the paper are very encouraging and promising due to low differences, the use of the prototype encoded in Matlab still constitutes an important technical limitation to work on larger urban areas. A test has been done on the Meyrin area enlarged to 1 km^2, but lowering the scene point resolution to 1 m, as well

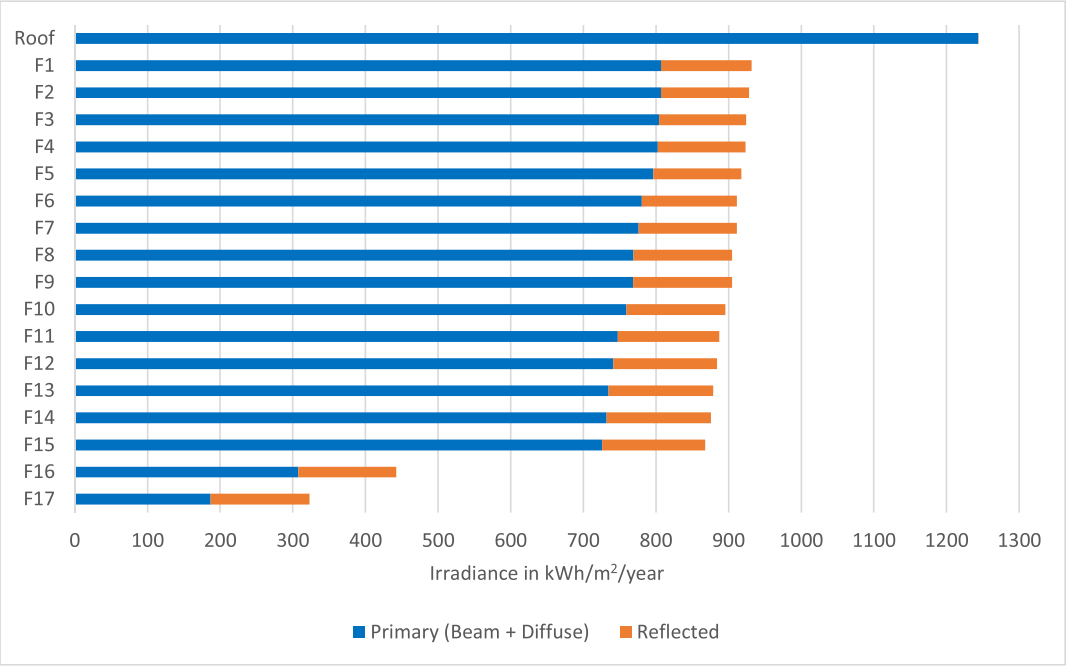

Fig. 21. Yearly irradiance profile in absolute values along a façade (1 m intervals) the distinguishing the contribution of the primary irradiance (in blue) and that of the reflection (in orange).

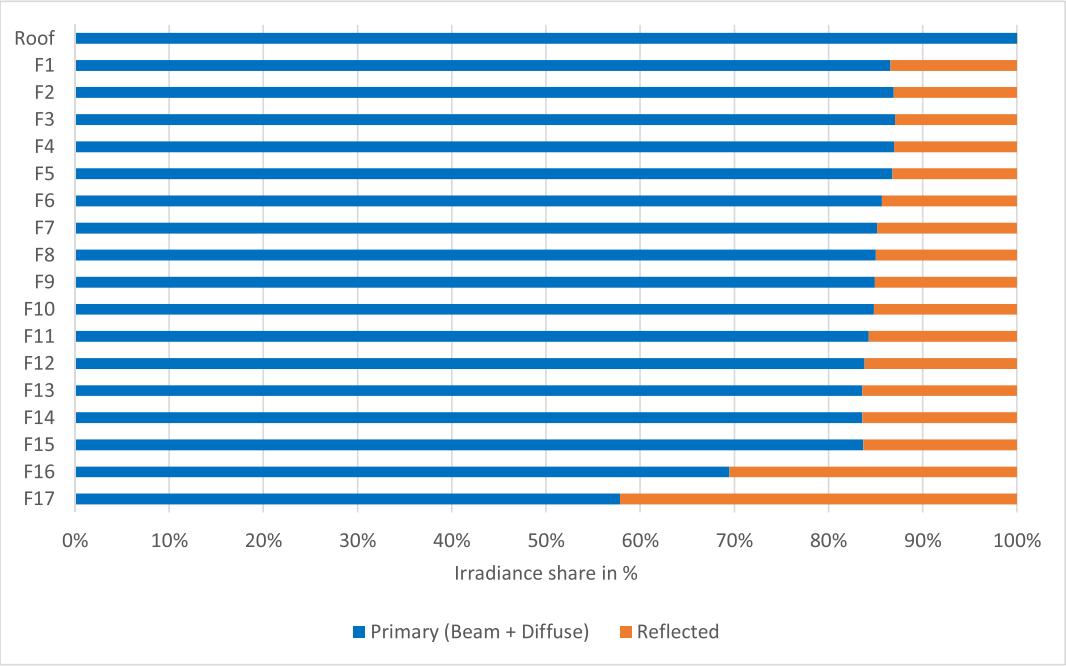

Fig. 22. Yearly irradiance profile in relative values.

as that of the sky (324 sky meshes instead of 2968 initially). The computing time was about 24 h, which remains rather prohibitive. However, using the same calculation base on Matlab with the classical radiosity method, processing such an area would simply not have been possible, neither on the smaller area of 300 m x 300 m with high resolution.

This therefore highlights two technical issues in order to calculate irradiance over a much larger area: the computation time and the memory storage (form factors) which both depends on the resolution of the scene points and the sky points. Detailed sensibility and robustness analyses should be performed in the next step in order to find the best compromise between scene points' resolution, reasonable memory storage, calculation time and sufficiently reliable results. Next step, a major mean to reduce calculation time will be particularly to implement the algorithms of reflection from Matlab to C++ language using GPU machines. This will be done in the same ways as with the original CadSol model for computing primary irradiance (I_G^0) and reflection based on the macro approach of Iqbal [24] at the scale of the Greater Geneva (2000 km^2, working by tile of 3.2 × 3.2 km, 1 to 1.5 h by tile calculation). Therefore, using computing improved performance, we will be able to process large urban scales with the R-CadSol model working tile by tile (of 1 km^2 or

even more) and complete the solar cadaster of Geneva with the facade component.

At the neighborhood scale, the solar potential can be extracted for all scene points at each time step, showing the advantages and disadvantages of different areas (roofs, facades or even ground) to install PV modules. As an example, the south facade of buildings in Meyrin presents more potential from October to March, which highlights the interest in facades for increasing the solar energy production in winter.

Based on the R-CadSol model introduced in the paper, further more detailed analyses could be carried out on the following issues in order to move towards concrete solar PV installations on building facades:

- Identification of structural and architectural surfaces on facades making photovoltaic installations optimal or not, working on improving the level of detail (LOD) based on 3D building models and terrestrial or aerial imagery.
- Esthetic criteria as the perception and the appearance of a whole neighborhood equipped with solar systems, also considering heritage issues, working on the solar panel integration and the adapted technologies (solar panels of different colors for instance).

Such analyses are particularly relevant in the current context, where we are moving towards making the most of all available surfaces in the urban environment.

Conflict of interest

All authors declare that they have no conflicts of interest.

Declaration of Competing Interest

None.

Acknowledgment

The authors would like to thank the HES-SO - University of Applied Sciences and Arts Western Switzerland (faculty of Engineering and Architecture) that funded the project VALES in which the presented model R-CadSol was developed. Part of the study was also cofounded by SIG - Industrial Services of Geneva (Fonds Vitales Environement). The authors would also like to thank the partners from the School of Engineering and Management (HEIG-VD) that contribute to the VALES working on 3D urban modeling and photogrammetry for windows detection, and the partners from NTNU (Norwegian University of Science and Technology) for academic exchanges in the field solar modeling in urban environment through the project HELIOS.

References

[1] N. Jolissaint, R. Hanbali, J.-.C. Hadorn, A. Schüler, Colored solar façades for buildings, Energy Procedia 122 (2017) 175–180, doi:10.1016/j.egypro.2017.07.340.
[2] B. Riedel, P. Messaoudi, Y.B. Assoa, P. Thony, R. Hammoud, L.-.E. Perret-Aebi, J.A. Tsanakas, Color coated glazing for next generation BIPV: performance vs aesthetics, EPJ Photovolt. 12 (2021) 11, doi:10.1051/epjpv/2021012.
[3] L. Romero Rodriguez, R. Nouvel, E. Dumini, U. Eicker, Setting intelligent city tiling strategies for urban shading simulations, Sol. Energy 157 (2017) 880–894, doi:10.1016/j.solener.2017.09.017.
[4] N. Stendardo, G. Desthieux, N. Abdennadher, P. Gallinelli, GPU-enabled shadow casting for solar potential estimation in large Urban areas. Application to the solar cadaster of greater Geneva, Appl. Sci. 10 (2020) 5361, doi:10.3390/app10155361.
[5] G. Desthieux, C. Carneiro, R. Camponovo, P. Gallinelli, N. Abdennadher, E. Morello, P. Leverington, A. Susini, C. Anthoine-Bourgeois. 2018a. Solar cadaster as a decision support tool for sustainable energy management in urban areas. From the State of Geneva to the cross-border Agglomeration. September 10.
[6] G. Desthieux, C. Carneiro, R. Camponovo, P. Ineichen, E. Morello, A. Boulmier, N. Abdennadher, S. Dervey, C. Ellert, Solar energy potential assessment on rooftops and facades in large built environments based on LiDAR data, image processing, and cloud computing. methodological background, application, and validation in Geneva (Solar Cadaster), Front. Built Environ. 4 (2018) 14, doi:10.3389/fbuil.2018.00014.
[7] D. Robinson, A. Stone, Solar radiation modelling in the urban context, Sol. Energy 77 (2004) 295–309, doi:10.1016/j.solener.2004.05.010.
[8] S.S. Nayak, V. Sharma. 2019. Technical paper on use of smart urban simulation software – 'CitySIM' for creation of smart cities in developing countries. 06, 5.
[9] D. Groleau. 2000. SOLENE un outil de simulation des éclairement solaires et lumineux dans les projets architecturaux et urbains. Proc. Les professionnels de la Construction - Confort intérieur: Outils informatiques d'aide à la conception et à la prévision du confort thermique, acoustique et d'éclairage rapport de recherche, Rouen 10-11 février 2000, CERMA.
[10] M. Musy, L. Maly, B. Morille, C. Inard, The use of SOLENE-microclimat model to assess adaptation strategies at the district scale, Urban Clim. Cooling Heat Islands 14 (2015) 213–223, doi:10.1016/j.uclim.2015.07.004.
[11] M. Sadeghipour Roudsari, M. Pak, Ladybug: a parametric environmental plugin for grasshopper to help designers create an environmentally-conscious design, in: Proceedings of the BS2013: 13th Conference of International Building Performance Simulation Association, 2013, pp. 3128–3135.
[12] G. Lobaccaro G, F. Frontini, G. Masera, T. Poli, SolarPW: a new solar design tool to exploit solar potential in existing urban areas, Energy Procedia 30 (2012) 1173–1183 [.
[13] T. Dogan, C.F. Reinhart, M. Panagiotis, Urban Daylight Simulation Calculation Calculating the Daylit Area of Urabn Designs, Presented at the IBPSA USA, Madison, 2012.
[14] C.F. Reinhart, T. Dogan, J.A. Jacubiek, R. Tarek, A. Swang, Umi – an urban simulation environment for building energy use, daylighting and walkability, in: Proceedings of the 13th Conference of International Building Performance Simulation Association, Chambéry (France), Massachusetts Institute of Technology, Department of Architecture, 2013, pp. 476–483.
[15] C.S. Good, G. Lobaccaro, S. Hårklau, Optimization of solar energy potential for buildings in Urban areas – a Norwegian case study, in: Proceedings of the Energy Procedia, Renewable Energy Research Conference, RERC 2014, 58, 2014, pp. 166–171, doi:10.1016/j.egypro.2014.10.424.
[16] G. Lobaccaro, S. Chatzichristos, V.A. Leon, Solar optimization of housing development, in: Proceedings of the Energy Procedia, 4th International Conference on Solar Heating and Cooling for Buildings and Industry (SHC 2015), 91, 2016, pp. 868–875, doi:10.1016/j.egypro.2016.06.253.
[17] Solemma, ClimateStudio, https://www.solemma.com/climatestudio (accessed 6 October 2022)
[18] Tracesoftware, Archelios suite, https://www.trace-software.com/archelios-suite/photovoltaic-pv-design-software/ (accessed 6 October 2022)
[19] Smart City Energy Platform, https://smartcity-energy.list.lu/#/home (accessed 9 November 2022)
[20] D. Koster, F. Minette, C. Braun, O. O'Nagy, Short-term and regionalized photovoltaic power forecasting, enhanced by reference systems, on the example of Luxembourg, Renew. Energy 132 (2019) 455–470, doi:10.1016/j.renene.2018.08.005.
[21] Ladybug Tools, https://www.ladybug.tools/ (accessed 6 October 2022)
[22] M.C. Brito, P. Redweik, C. Catita, S. Freitas, M. Santos, 3D solar potential in the urban environment: a case study in Lisbon, Energies 12 (2019) 3457, doi:10.3390/en12183457.
[23] B. Govehovitch, M. Thebault, K. Bouty, S. Giroux, E. Peyrol, V. Guillot, C. Ménézo, G. Desthieux, Numerical validation of the radiative model for the solar cadaster developed for greater Geneva, Appl. Sci. 11 (2021) 8086, doi:10.3390/app11178086.
[24] M. Iqbal, An Introduction To Solar Radiation - 1st Edition, 1st Ed., Academic Press, 1983 ed.
[25] B. Raybaud, Evaluation De L'impact Des Propriétés Optiques Large-Bande De L'environnement Sur Le Productible (énergie incidente) En Milieu Urbain (phdthesis), Université de Lyon, 2020.
[26] M. Thebault, B. Govehovitch, K. Bouty, C. Caliot, R. Compagnon, G. Desthieux, M. Formolli, S. Giroux-Julien, V. Guillot, E. Herman, J. Kämpf, J. Kanters, G. Lobaccaro, C. Ménézo, G. Peronato, A.J. Petersen, A comparative study of simulation tools to model the solar irradiation on building façades, in: Proceedings of the Solar World Congress, International Solar Energy Society, 2021, doi:10.18086/swc.2021.38.04.
[27] M. Thebault M, G. Desthieux, R. Castello, L. Berrah, Large-scale evaluation of the suitability of buildings for photovoltaic integration: case study in Greater Geneva, Appl. Energy 316 (2022) 119127, doi:10.1016/j.apenergy.2022.119127.
[28] Web application of the solar cadaster of the Greater Geneva https://apps.sitg-lab.ch/solaire/ (accessed 6 October 2022)
[29] C. Ratti, Urban Analysis For Environmental Prediction, University of Cambridge Department of Architecture, Cambridge, 2001.
[30] J.E. Hay, Calculation of monthly mean solar radiation for horizontal and inclined surfaces, Sol. Energy 23 (1979) 301–330, doi:10.1016/0038-092X(79)90123-3.
[31] J. Widén, J. Munkhammar, Solar Radiation Theory, Uppsala University, 2019, doi:10.33063/diva-381852.
[32] M. Patriarche. 2014. Mesure et modélisation de la lumière naturelle dans les canyons urbains (phdthesis). École Nationale des Travaux Publics de l'État [ENTPE].
[33] W. Nusselt, Graphische bestimmung des winkelverhaltnisses bei der wrmestrahlung, Z. Vereines Dtsch. Ingenieure, VDI Z. 72 (1928) 673.
[34] M. Cohen, D. Greenberg, 1985. The hemi-cube: a radiosity solution for complex environments. SIGGRAPH 85 Conf. Proc. July 1985 Vol 19 No 3 Pp 31-39 Ill Some Col Incl. Bibliogr. 19.
[35] J.E. Hilton, Dynamic modelling of radiant heat from wildfires, in: Proceedings of the 22nd International Congress on Modelling and Simulation, Hobart, Tasmania, Australia, 2017 3 to 8 December 2017.
[36] B. Raybaud, E. Vergnault, A. Disdier, P. Thony, J.-.J. Roux, Identification of BRDF parameters with spectral measurements in the visible light spectrum towards solar irradiation evaluation in urban environment for photovoltaïc technologies, Energy Build. 263 (2022) 112034, doi:10.1016/j.enbuild.2022.112034.

[37] H.E. Rushmeier, K.E. Torrance, Extending the radiosity method to include specularly reflecting and translucent materials, ACM Trans. Graph. 9 (1990) 1–27, doi:10.1145/77635.77636.
[38] N.L. Alchapar, E.N. Correa, 6 - Comparison of the performance of different facade materials for reducing building cooling needs, in: F. Pacheco-Torgal, J.A. Labrincha, L.F. Cabeza, C.G. Granqvist (Eds.), Eco-Efficient Materials for Mitigating Building Cooling Needs, Woodhead Publishing, Oxford, 2015, pp. 155–194, doi:10.1016/B978-1-78242-380-5.00006-6.
[39] İ. Yildiz, 1.15 solar energy, in: I. Dincer (Ed.), Comprehensive Energy Systems, Elsevier, Oxford, 2018, pp. 638–664, doi:10.1016/B978-0-12-809597-3.00117-6.